NASA MEMO 6-14-59L

NASA

MEMORANDUM

DETERMINATION OF STATIC STRENGTH AND CREEP BUCKLING OF UNSTIFFENED CIRCULAR CYLINDERS SUBJECTED TO BENDING AT ELEVATED TEMPERATURES

By Eldon E. Mathauser and Avraham Berkovits

Langley Research Center
Langley Field, Va.

NATIONAL AERONAUTICS AND SPACE ADMINISTRATION
WASHINGTON
June 1959

NATIONAL AERONAUTICS AND SPACE ADMINISTRATION

MEMORANDUM 6-14-59L

DETERMINATION OF STATIC STRENGTH AND CREEP BUCKLING OF UNSTIFFENED CIRCULAR CYLINDERS SUBJECTED TO BENDING AT ELEVATED TEMPERATURES

By Eldon E. Mathauser and Avraham Berkovits

SUMMARY

A method based on a semiempirical procedure is presented for predicting static strength and creep buckling of unstiffened circular cylinders subjected to pure bending at elevated temperatures. The method is applicable to cylinders that are loaded into the inelastic stress range prior to buckling and fail in a local mode. The predicted bending moments associated with static strength and creep buckling are compared with experimental data (taken from NACA RM 57E17) obtained from tests at 500° F on 5052-0 aluminum-alloy cylinders with radius-thickness ratios ranging from 125 to 250.

INTRODUCTION

The development of semiempirical methods of analysis applicable to the determination of static strength and creep buckling of structural components at elevated temperatures has been the object of several studies made by the NASA (formerly NACA). A summary of some of these studies is given in reference 1. These studies were concerned with the elevated-temperature behavior of various structural components but did not include unstiffened circular cylinders. In view of the importance of cylinders in structural applications at elevated temperatures, some investigations of cylinder behavior at elevated temperature have been made recently by several investigators. Studies of elevated-temperature strength and creep buckling of axially compressed cylinders are reported in references 2 and 3. Experimental strength and creep buckling results from unstiffened circular cylinders subjected to pure bending at elevated temperatures are given in reference 4.

In the present paper, the semiempirical methods of analysis presented in reference 1 are applied in the determination of elevated-temperature static strength and creep buckling of unstiffened circular

cylinders subjected to pure bending and loaded into the inelastic stress range prior to buckling. The bending strength of the cylinders is determined on the basis of an existing local buckling stress relationship and the compressive stress-strain curve for the material. Creep buckling is determined in a similar manner with the use of isochronous stress-strain curves obtained from compressive creep data. The predicted results are compared with the experimental data given in reference 4. The prediction of creep buckling stresses from stresses associated with either experimental or calculated static strength of the cylinders is discussed.

SYMBOLS

A	area, sq in.
E	Young's modulus, ksi
E_s	secant modulus, ksi
E_t	tangent modulus, ksi
k	buckling coefficient
M	bending moment, in-kips
n	total number of elements
r	radius, in.
t	thickness, in.
y	perpendicular distance from axis of bending to element of area in cylinder, in. (see fig. 3)
ϵ	strain
σ	stress, ksi
σ_{cr}	local buckling stress, ksi
τ	time, hr
η	plasticity reduction factor

Subscript:

i	pertains to element

METHOD OF ANALYSIS

Static Strength

In the present study, the determination of the static bending strength of cylinders is made on the basis of the following equation which defines the elastic local buckling stress for axially compressed cylinders:

$$\sigma_{cr} = kE\frac{t}{r} \tag{1}$$

where k is the buckling coefficient and has a theoretical value of approximately 0.6, E is the elastic or Young's modulus, and t/r is the thickness-radius ratio of the cylinder. Equation (1) was derived for axially compressed cylinders (ref. 5) and has often been used to determine local buckling stresses for cylinders subjected to bending. Experimental results indicate that the buckling coefficient k is not a constant but, rather, is dependent on the radius-thickness ratio of the cylinder. (For example, see ref. 6.) Furthermore, for cylinders stressed into the inelastic range of the material prior to buckling, the elastic modulus E in equation (1) is replaced by an effective modulus ηE as follows:

$$\sigma_{cr} = k\eta E\frac{t}{r} \tag{2}$$

Different material parameters have been assumed for the plasticity reduction factor η; for example, E_t/E, in reference 2 and E_s/E, in reference 3. In the present study, η is assumed to be given by the parameter $\sqrt{E_tE_s}/E$, which is a simplified approximation for the plasticity reduction factor given in reference 7. Equation (2) may thus be written as

$$\sigma_{cr} = k\sqrt{E_tE_s}\frac{t}{r}$$

where E_t and E_s are evaluated from the material stress-strain curve at the stress σ_{cr}.

Equation (2) is assumed to define the extreme-fiber local buckling stress for cylinders subjected to pure bending and is applicable if buckling occurs in either the elastic or inelastic stress ranges of the material at room or elevated temperatures. The buckling stress is also assumed to be equivalent to the maximum extreme-fiber bending stress

that can be applied on the unstiffened circular cylinders. This assumption, in general, is in good agreement with experience. In addition, it is assumed that no local deformations occur prior to buckling and that the strain distribution is linear over the cross section of the cylinder in both the elastic and inelastic stress ranges of the material.

The solution for the buckling stress of cylinders loaded into the inelastic stress range from equation (2) can be accomplished conveniently with the aid of a plot such as shown in figure 1. The solid curve determined from the material stress-strain curve indicates the variation of σ with $\sigma/\eta E$, where $\eta E = \sqrt{E_t E_s}$. The dashed line indicates a constant value of $k\frac{t}{r}$. The stress defined by the intersection of the solid and dashed curves gives the extreme-fiber buckling stress σ_{cr} for the cylinder.

The magnitude of the buckling moment associated with the extreme-fiber buckling stress is generally of interest. If the cylinder is loaded into the inelastic stress range prior to achieving σ_{cr}, the relationship between the applied bending moment and the extreme-fiber stress becomes nonlinear as shown, for example, in figure 2. In this method of analysis, the magnitude of the moment corresponding to an inelastic extreme-fiber stress is determined by a numerical procedure. The numerical procedure discussed in the following paragraph is based on the assumption that the tensile and compressive stress-strain curves are similar. Modifications to this procedure for dissimilar tensile and compressive material properties are described subsequently.

In the numerical analysis, the cylinder is subdivided into 40 elements of equal area. A quadrant of the cylinder indicating this subdivision is shown in figure 3. Forty elements were selected on the basis of a preliminary study which indicated that adequate accuracy for the purpose of this analysis was obtained with this number of elements. For a given extreme-fiber stress, the magnitude of the stresses in all other elements is defined from the material stress-strain curve by making use of the assumption that a linear strain distribution exists in the cylinder. The magnitude of the bending moment corresponding to the defined stress distribution is obtained from the moment equilibrium equation

$$\int \sigma y \, dA = M \tag{3}$$

which is written as follows for use in the numerical procedure:

$$\sum_{i=1}^{n} \sigma_i y_i A_i = M \tag{4}$$

where σ_i defines the stress in an element, y_i defines the perpendicular distance from the axis of bending (see fig. 3) to the element, and A_i is the area of the element. Equation (4) may then be solved by taking σ_i in the extreme fiber equal to σ_{cr} determined from equation (2). The solution for the static bending strength is thus complete inasmuch as figure 1 defines the extreme-fiber buckling stress and equation (4) defines the buckling moment corresponding to this stress.

When the tensile and compressive stress-strain curves are not similar, an additional equation involving thrust equilibrium is required for determination of the relationship between M and σ. The equation is

$$\int \sigma \, dA = 0 \tag{5}$$

which may be written for the numerical procedure as follows:

$$\sum_{i=1}^{n} \sigma_i A_i = 0 \tag{6}$$

The magnitude of the moment corresponding to a given extreme-fiber compressive stress σ_{cr} is obtained by solving equations (4) and (6) simultaneously by an iterative or successive approximations procedure. This method of analysis also defines the neutral or bending axis for the cylinder.

Creep Buckling

The determination of the bending moments that produce creep buckling of circular cylinders is based on the method outlined previously for predicting static strength. Isochronous stress-strain curves derived from material creep data are substituted for the material stress-strain curves to predict the extreme-fiber creep buckling stresses from equation (2). The bending moments corresponding to the extreme-fiber creep buckling stresses are determined from equation (4) for similar tensile and compressive creep properties and from equations (4) and (6) for different tensile and compressive creep properties.

EXPERIMENTAL RESULTS

Cylinder Data

The experimental data given in reference 4 on the elevated-temperature static strength and creep buckling of circular cylinders were used as a basis for comparison with the results predicted by the methods outlined in the present study. The test specimens reported in reference 4 were unstiffened circular cylinders 48 inches long and 16 inches in diameter. These specimens were fabricated from 5052-O aluminum-alloy sheets with nominal skin thicknesses of 0.064, 0.051, 0.040, and 0.032 inch. These skin thicknesses correspond to nominal radius-thickness ratios of 125, 157, 200, and 250, respectively. The cylinders were subjected to pure bending at room temperature and 500° F to determine static strength and were also subjected to constant moments at 500° F to determine creep lifetimes. The results of both the strength and creep tests are presented and discussed in the section entitled "Comparison Between Predicted and Experimental Results."

Material Stress-Strain Data

No materials data were given in reference 4 for the 5052-O aluminum-alloy sheets. In order that comparison between the experimental and calculated results could be made, tensile and compressive stress-strain and creep tests were performed on this material for sheet thicknesses of 0.064 inch and 0.032 inch. These tests were made in both the with-grain and cross-grain directions of the sheets. The tensile and compressive stress-strain results are given in figure 4. These data were obtained from the 0.064-inch-thick sheet tested in the with-grain direction. The specimens were exposed to the test temperature for 30 minutes prior to loading. No significant differences were obtained from tests in the cross-grain direction for this sheet thickness or from tests in either grain direction of the 0.032-inch-thick sheet. It was thus concluded that the stress-strain properties for the 5052-O aluminum-alloy sheet were essentially independent of grain direction and were also independent of sheet thickness.

Material Creep Data

Tensile and compressive creep tests were performed on the 5052-O aluminum-alloy sheet to provide material creep data for the determination of cylinder lifetime. The results of these material creep tests are shown in figure 5. The curves in figures 5(a) and 5(b) indicate tensile creep results obtained from sheets tested in the with-grain direction at 500° F. Results for 0.064-inch-thick and 0.032-inch-thick sheets are indicated. These material specimens were exposed to

the 500° F test temperature for 30 minutes prior to the application of the constant load in a tensile creep testing machine. Similar results were obtained from the tensile creep tests on the material in the cross-grain direction.

Figure 5(c) indicates the compressive creep test results which were obtained from the 0.064-inch-thick sheet tested in the with-grain direction. The compressive creep specimens were tested in a V-groove edge-support fixture and were also exposed to the 500° F test temperature for 30 minutes prior to application of the constant load. In view of the similar material properties obtained from the stress-strain tests in the with-grain and cross-grain directions, no compressive creep tests were performed on the 0.064-inch-thick sheet in the cross-grain direction or on the 0.032-inch-thick sheet in either grain direction.

A cross plot of the compressive creep data given in figure 5(c) at constant times gives the isochronous compressive stress-strain curves shown as solid curves in figure 6. The isochronous compressive stress-strain curves indicate the strain produced immediately on application of a given stress plus the creep strain obtained at that stress for the indicated times. The dashed curve (labeled σ-ϵ) shown for comparison purposes is the compressive stress-strain curve taken from figure 4 for the material at 500° F.

COMPARISON BETWEEN PREDICTED AND EXPERIMENTAL RESULTS

Static Strength

The predicted extreme-fiber buckling stresses appropriate to the four radius-thickness ratios of the test cylinders are indicated in figure 7 by the intersections of the solid and dashed lines. The solid curve in this figure indicates the variation of σ with $\sigma/\eta E$ obtained from the compressive stress-strain curve (fig. 4) at 500° F. The dashed lines indicate constant values of $k\frac{t}{r}$ which are applicable to the four radius-thickness ratios of the test cylinders. The magnitude of the buckling coefficient k was taken from figure 8. This variation of k with radius-thickness ratio was evaluated from reference 6 and is appropriate for unstiffened cylinders subjected to bending.

The magnitude of the bending moments that correspond to the extreme-fiber buckling stresses indicated in figure 7 was calculated from equation (4). These moments are indicated by the end points of the curves given in figure 9. The variation of M with σ is shown for all values of extreme-fiber stress up to σ_{cr}. The relationship between M and σ

is linear up to an extreme-fiber stress of approximately 7 ksi, which corresponds to the proportional limit stress for the material at 500° F. (See fig. 4.) Above 7 ksi, the variation of M with σ becomes nonlinear; however, the deviation from linearity is small, particularly for the cylinders with the high radius-thickness ratios.

A comparison between the experimental and predicted strengths of the cylinders at 500° F is given in figure 10. For radius-thickness ratios of 157 and 200, satisfactory agreement between the experimental and calculated results was generally obtained. For radius-thickness ratios of 125 and 250, the predicted moments exceed the experimental values. No attempt was made to compare the experimental and predicted strengths at room temperature. The room-temperature stress-strain curve is characterized by a flat top at the initiation of inelastic action in the material. For this type of stress-strain curve, the magnitude of the inelastic extreme-fiber buckling stress is defined; however, the magnitude of the corresponding strain is indeterminate. In view of the indeterminate magnitude of the strain in the extreme fiber, the stress distribution over the cross section of the cylinder is unknown and the use of equation (4) for the determination of the bending moment is precluded.

Creep Buckling

The bending moments which produce creep buckling of the cylinders for radius-thickness ratios appropriate to the test data of reference 4 were predicted from the method outlined previously for determination of static strength. Isochronous stress-strain curves were substituted for the material stress-strain curves in the calculations. The initial calculation was based on compressive creep data only and is described in the following paragraph. Calculations based on tensile creep data only as well as calculations based on both tensile and compressive creep data were also made and are discussed subsequently.

The extreme-fiber compressive stresses that produce creep buckling in various times were obtained from figure 11. The solid curves indicate the variation of σ with $\sigma/\eta E$ obtained from the isochronous stress-strain curves shown in figure 6. The dashed lines in figure 11 are constant values of $k\frac{t}{r}$ which are applicable to the indicated radius-thickness ratios. (The values of the buckling coefficient k were taken from fig. 8.) The bending moments corresponding to the extreme-fiber creep buckling stresses are indicated by the end points of the curves in figure 12. The bending moments were calculated from equation (4) and the isochronous stress-strain curves in figure 6. The variation of M with σ is shown for all values of extreme-fiber stress up to σ_{cr}. Although the relationship between M and σ is nonlinear,

the deviation from linearity is small and compares approximately with the deviations obtained from the static strength calculations shown in figure 9. The creep buckling moments indicated in figure 12 are compared with the experimental results in figure 13. For lifetimes less than 0.2 hour, the experimental creep buckling moments are generally less than the predicted moments. For longer lifetimes, the experimental moments exceed the predicted moments.

Calculations for creep buckling moments based on tensile creep data only were made for purposes of comparison with the previous calculations based solely on compressive creep data. The buckling moments predicted from the tensile creep data parallel the results obtained from the compressive creep data shown in figure 13, and, in general, were approximately 20 percent less than the buckling moments obtained from the compressive creep data alone. These results were anticipated on the basis of a comparison between the tensile and compressive creep data plotted in the form of σ against $\sigma/\eta E$ as shown in figure 11. The tensile creep data yielded values of predicted buckling stress that were approximately 20 percent less than those obtained from the compressive creep data.

Calculations of creep buckling moments made on the basis of both tensile and compressive creep data were also made with the use of equations (2), (4), and (6). These predicted creep buckling moments again parallel the results obtained from the compressive creep data alone. The predicted buckling moments in this case were approximately 5 percent less than the corresponding buckling moments shown in figure 13. These calculations based on both tensile and compressive creep data did not improve the correlation between experimental and calculated creep buckling moments over that obtained from compressive creep data only. Furthermore, the computation for creep buckling was simplified considerably when made on the basis of compressive creep data only. Analysis for creep buckling based on both tensile and compressive creep data may be necessary only when considerably different tensile and compressive creep properties exist.

CONCLUDING REMARKS

An analysis based on a semiempirical procedure has been presented for predicting the elevated-temperature static buckling strength and the creep buckling strength of unstiffened circular cylinders subjected to bending. The determination of buckling stresses by this procedure is based on the observation that a shell structure of a given geometry appears to buckle at a stress corresponding to a constant value of $\sigma/\eta E$ regardless of material or test temperature, provided that a suitable expression for the plasticity reduction factor η is chosen (σ = Stress; E = Young's modulus). Comparison of the predicted results with experimental results (taken from NACA RM 57E17) obtained on 5052-0 aluminum-alloy

cylinders with radius-thickness ratios ranging from 125 to 250 indicates that this procedure is valid for determining the buckling stresses associated with either static strength or creep buckling of cylinders. Isochronous stress-strain curves are employed in this procedure for determination of the creep buckling stresses.

In view of the satisfactory correlation between the predicted and experimental static strength and creep buckling results, it appears that creep buckling stresses may be predictable solely from a knowledge of the static strength of the cylinders at the same or lower test temperatures and the appropriate material stress-strain and material creep data. Additional tests of cylinders fabricated from other materials and tested at several temperatures will help to determine the validity of this assumption.

Langley Research Center,
National Aeronautics and Space Administration,
Langley Field, Va., March 24, 1959.

REFERENCES

1. Heldenfels, Richard R., and Mathauser, Eldon E.: A Summary of NACA Research on the Strength and Creep of Aircraft Structures at Elevated Temperatures. NACA RM L56D06, 1956.

2. Baer, H. W.: Very Short Time Creep Buckling. Tech. Memo. No. 306 (Contract AF33(038)-28634), Res. and Dev. Labs., Hughes Aircraft Co., June 15, 1953.

3. Bozajian, J. M., and Tsao, C. H.: Creep Buckling of Cylindrical Shells in Axial Compression. SRSM7-196 (Contract Nos. AF33(038)-28634, AF33(600)-28438), Systems Dev. Labs., Hughes Aircraft Co., Dec. 1, 1957.

4. Erickson, Burton, Patel, Sharad A., French, Francis W., Lederman, Samuel, and Hoff, N. J.: Experimental Investigation of Creep Bending and Buckling of Thin Circular Cylindrical Shells. NACA RM 57E17, 1957.

5. Timoshenko, S.: Theory of Elastic Stability. McGraw-Hill Book Co., Inc., 1936.

6. Peterson, James P.: Weight-Strength Studies of Structures Representative of Fuselage Construction. NACA TN 4114, 1957.

7. Bijlaard, P. P.: Theory and Tests on the Plastic Stability of Plates and Shells. Jour. Aero. Sci., vol. 16, no. 9, Sept. 1949, pp. 529-541.

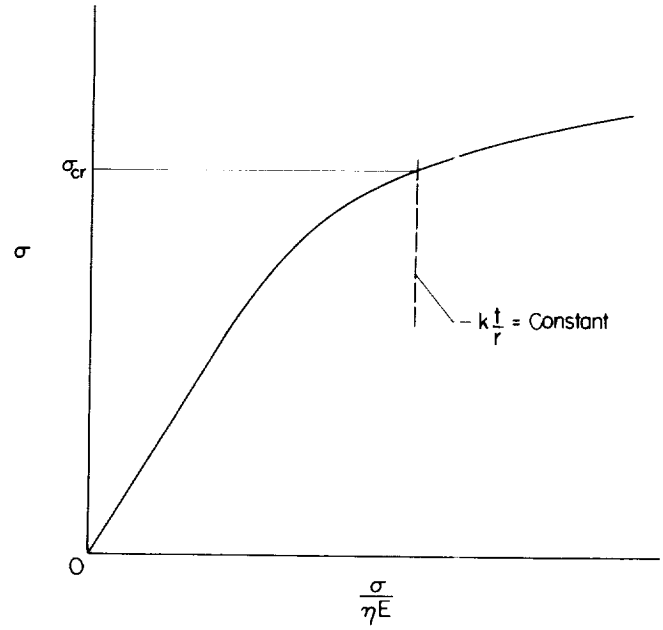

Figure 1.- Graphical solution for local buckling stress.

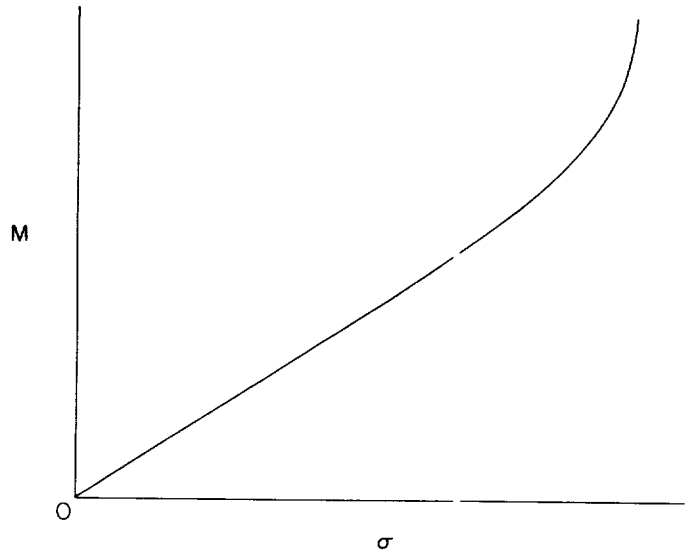

Figure 2.- Example of variation of applied moment with extreme-fiber stress for cylinder loaded into inelastic stress range prior to buckling.

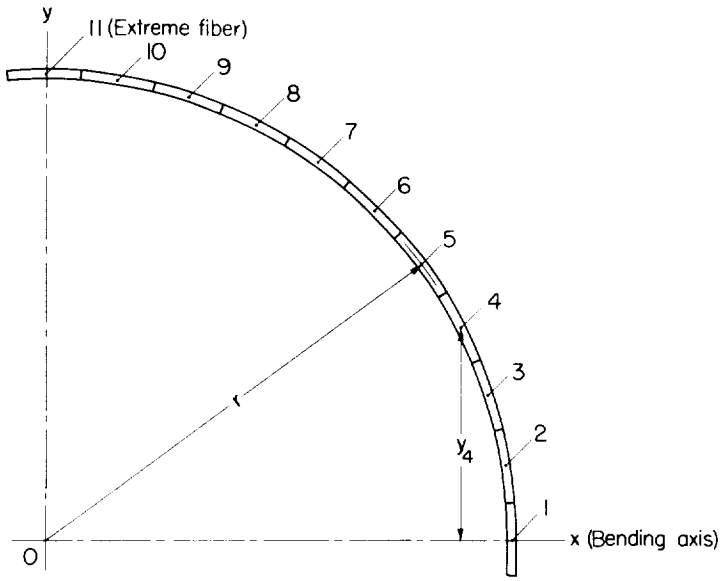

Figure 3.- Subdivision of cylinder into elements of equal area for numerical analysis.

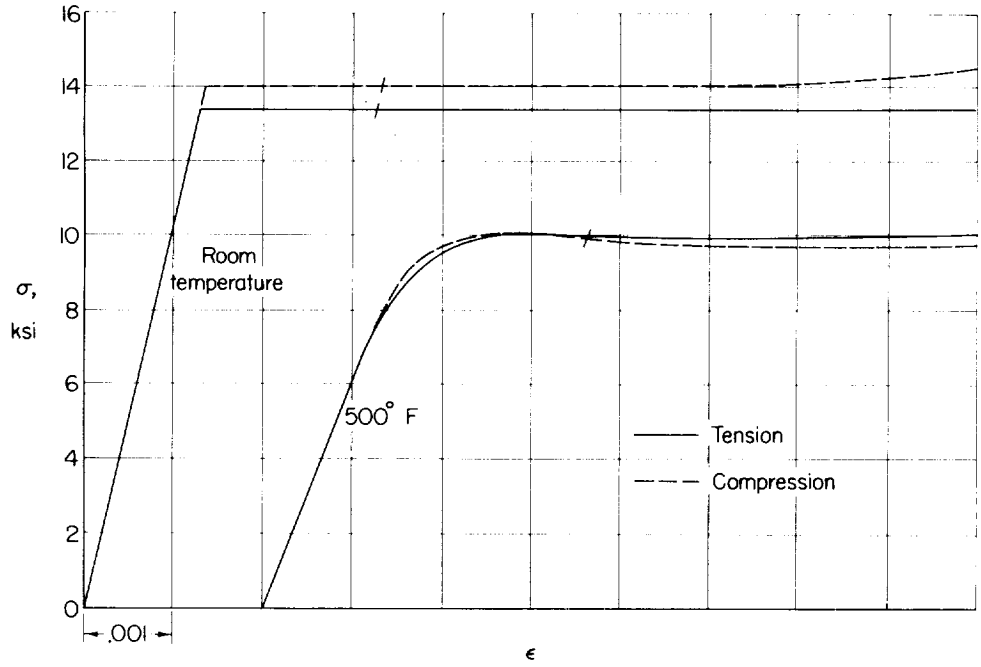

Figure 4.- Tensile and compressive stress-strain curves for 5052-0 aluminum-alloy sheet. Thickness, 0.064 inch; nominal strain rate, 0.002 per minute; exposed at 500° F for 30 minutes prior to loading in 500° F tests; tests performed in with-grain direction of sheet.

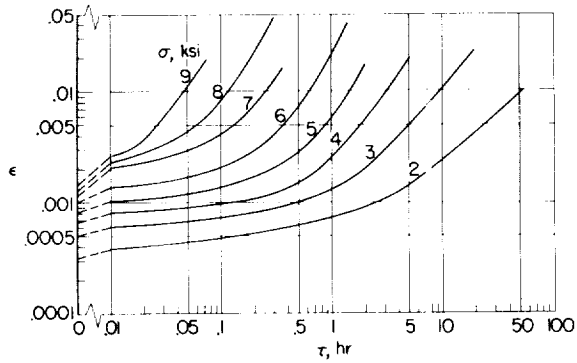

(a) Tensile creep curves; sheet thickness, 0.064 inch.

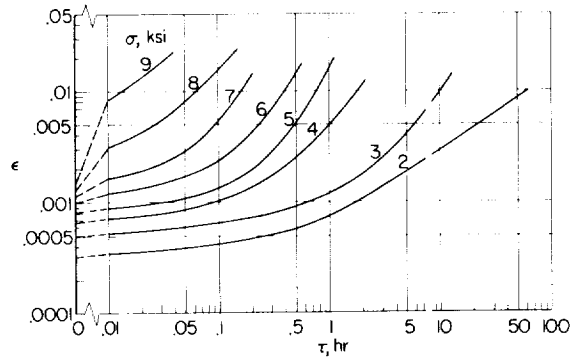

(b) Tensile creep curves; sheet thickness, 0.032 inch.

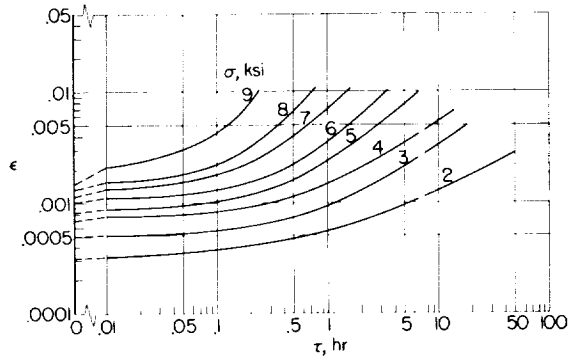

(c) Compressive creep curves; sheet thickness, 0.064 inch.

Figure 5.- Material creep curves for 5052-O aluminum-alloy sheet at 500° F. Exposed at 500° F for 30 minutes prior to loading; tests performed in with-grain direction of sheet.

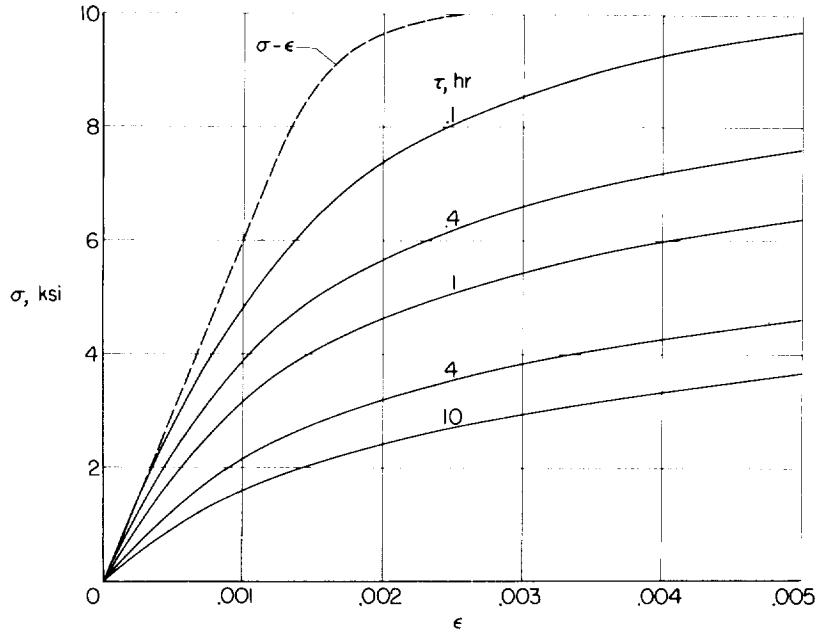

Figure 6.- Isochronous compressive stress-strain curves for 5052-0 aluminum-alloy sheet at 500° F.

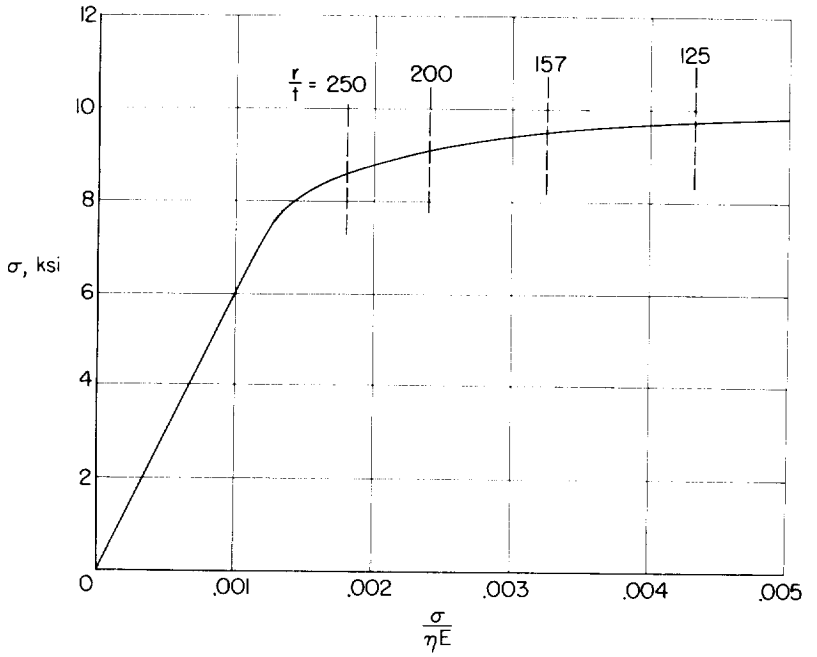

Figure 7.- Graphical solution for extreme-fiber buckling stresses for 5052-0 aluminum-alloy cylinders at 500° F.

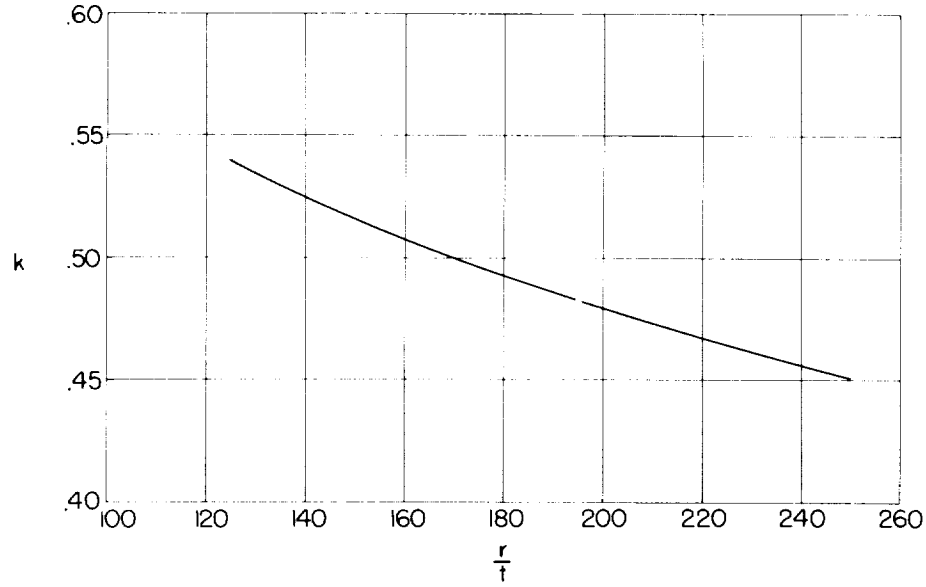

Figure 8.- Variation of local buckling coefficient with radius-thickness ratio for unstiffened circular cylinders subjected to bending. (Evaluated from ref. 6.)

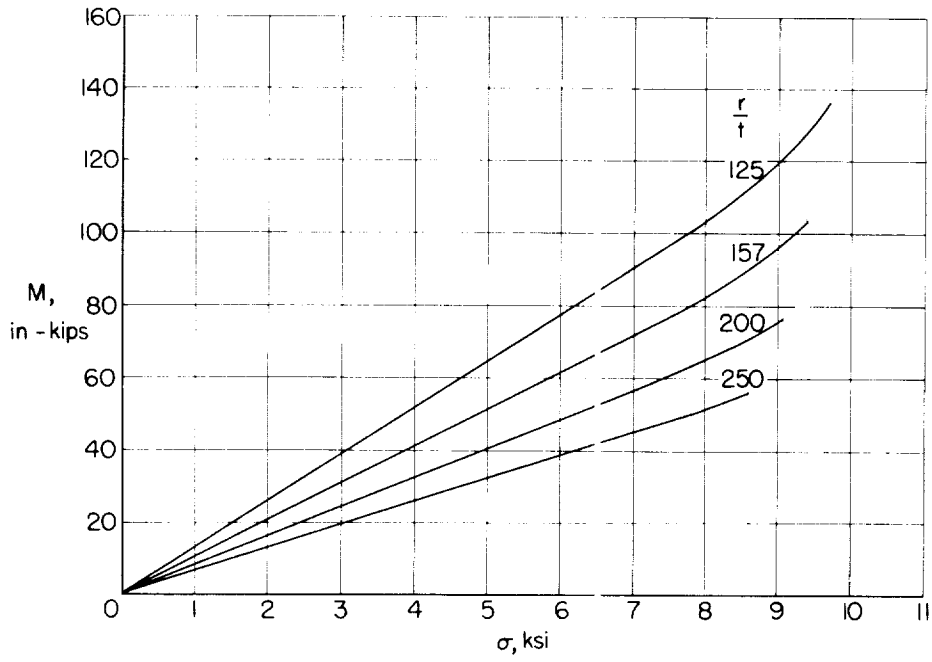

Figure 9.- Variation of applied moment with extreme-fiber compressive stress for 5052-0 aluminum-alloy cylinders at 500° F.

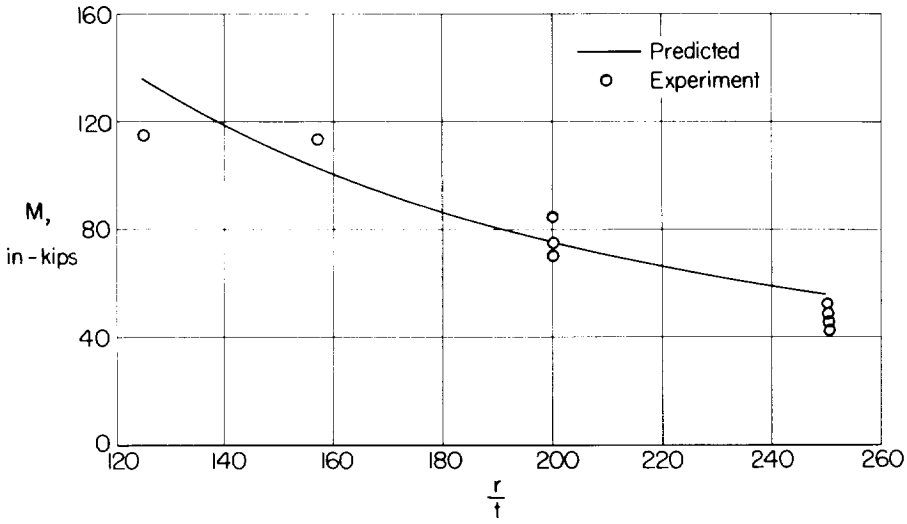

Figure 10.- Comparison between calculated and experimental buckling moments for 5052-0 aluminum-alloy cylinders at 500° F.

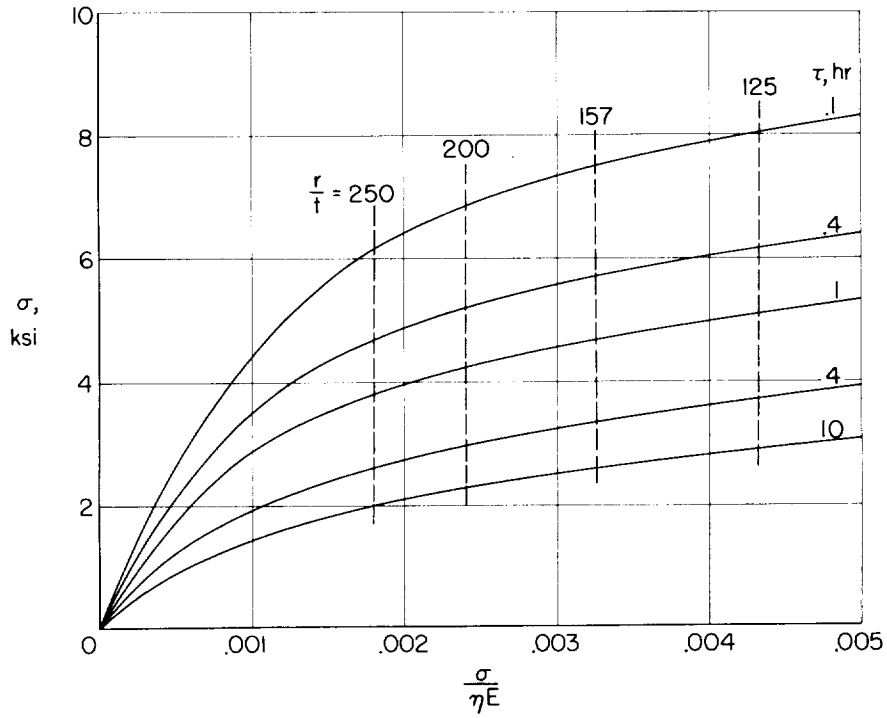

Figure 11.- Graphical solution for extreme-fiber compressive stresses that produce creep buckling of 5052-0 aluminum-alloy cylinders at 500° F.

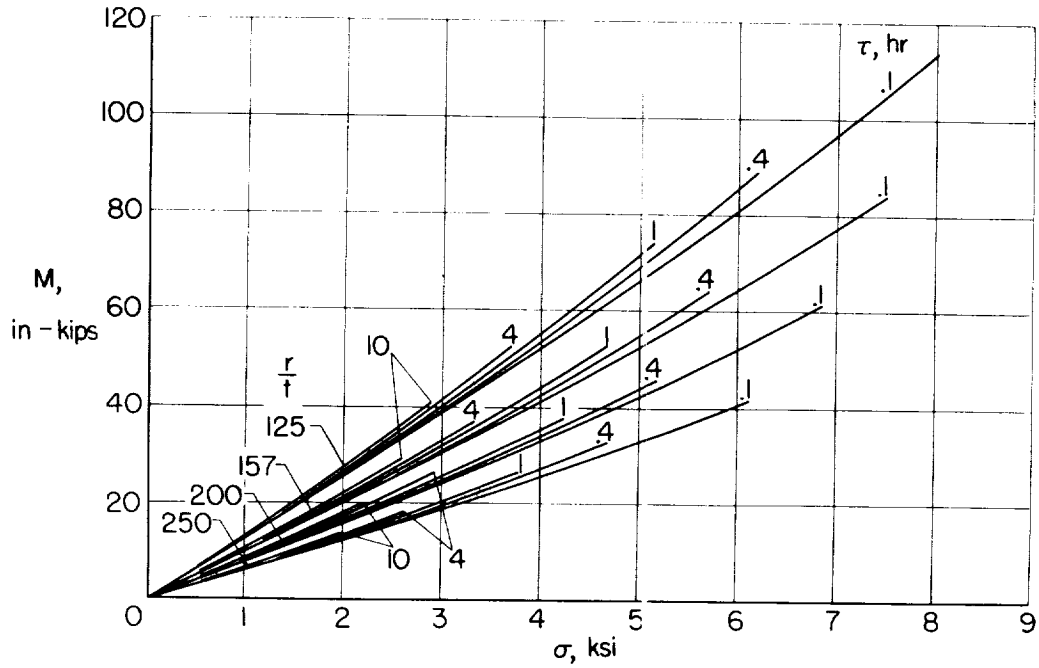

Figure 12.- Variation of applied moment with extreme-fiber compressive stress for 5052-0 aluminum-alloy cylinders at 500° F.

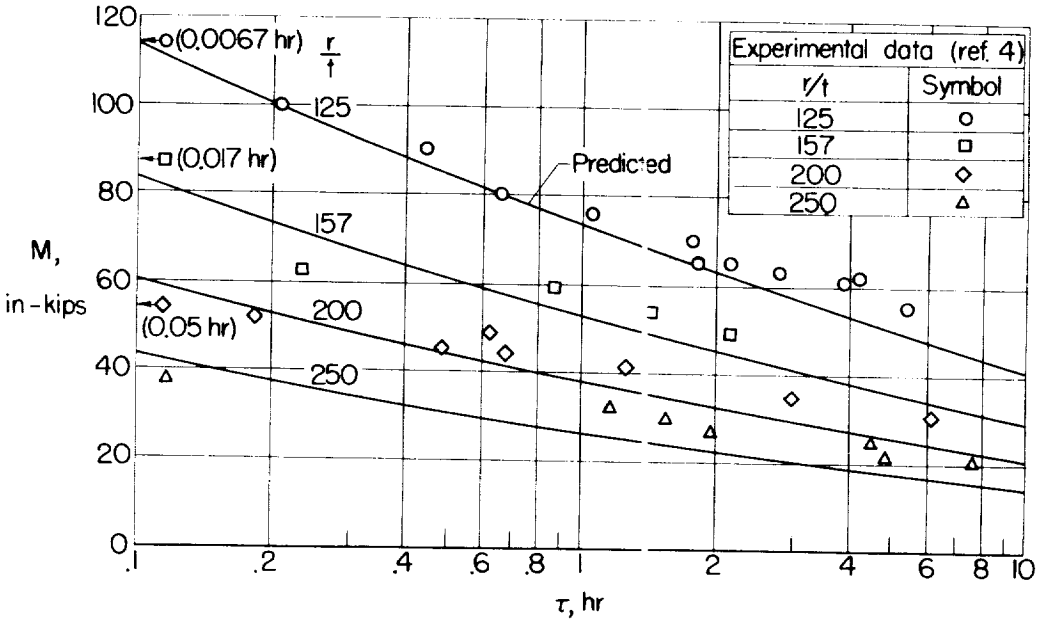

Figure 13.- Comparison between predicted and experimental creep buckling moments for 5052-0 aluminum-alloy cylinders at 500° F.